Research Square

Preprints are preliminary reports that have not undergone peer review.
They should not be considered conclusive, used to inform clinical practice,
or referenced by the media as validated information.

Elevated TGFβ1 Drives IL4I1⁺ Macrophage–Gal-9 Signaling to Shape Tumor-Specific CD8⁺ T- Cell States in COPD-Associated NSCLC

Mingshu Xiao
The Fourth Affiliated Hospital of Zhejiang University School of Medicine
Guoxin Cai
Zhejiang University
Yun Xu
The Fourth Affiliated Hospital of Zhejiang University School of Medicine
Xue Zhang
Zhejiang University
Yichang Chen
Zhejiang University
Ying Yang
The Fourth Affiliated Hospital of Zhejiang University School of Medicine
Yu Geng
The Fourth Affiliated Hospital of Zhejiang University School of Medicine
Min Zhang
The Second Affiliated Hospital of Zhejiang University School of Medicine
Zhan Zhou
The Fourth Affiliated Hospital of Zhejiang University School of Medicine
Kai Wang
The Fourth Affiliated Hospital of Zhejiang University School of Medicine
Jiangnan Zhao
0622222@zju.edu.cn

The Fourth Affiliated Hospital of Zhejiang University School of Medicine

Article

Keywords: COPD, non-small cell lung cancer, tumor immunology, single-cell atlas

Posted Date: May 4th, 2026

DOI: https://doi.org/10.21203/rs.3.rs-9365545/v1

License: This work is licensed under a Creative Commons Attribution 4.0 International License.
Read Full License

Additional Declarations: No competing interests reported.

Abstract

Chronic obstructive pulmonary disease (COPD)-associated non-small cell lung cancer (NSCLC) exhibits distinct responses to immune checkpoint blockade, indicating a unique tumor immune microenvironment. Here, we integrate single-cell transcriptomics and T cell receptor sequencing of tumor, adjacent non-tumor, and blood samples from NSCLC patients, together with spatial transcriptomics and molecular validation. We identify an immunosuppressive niche in COPD-associated NSCLC characterized by elevated TGFβ1 expression in malignant cells and enhanced crosstalk with IL4I1^{+} tumor-associated macrophages. Notably, macrophage-derived galectin-9 (Gal-9) modulates tumor-specific CD8^{+} T-cell states, promoting CXCL13 and CD82 expression within a proliferative, tumor-reactive subset, while also being associated with features of T-cell exhaustion. These findings define a TGFβ1–IL4I1^{+} macrophage–Gal-9 axis that reshapes CD8^{+} T-cell states and contribute to differential immunotherapy responses in COPD-associated NSCLC.

Introduction

The health burden of Chronic Obstructive Pulmonary Disease (COPD) has intensified, now ranking as the third leading cause of death worldwide[1]. Notably, a 2019 study revealed a 13.7% COPD prevalence among individuals aged 40 and above in China, affecting nearly 100 million people[2]. COPD is associated with a significantly higher risk of lung cancer (LC), with evidence indicating a 2.15-fold increased incidence of among patients with COPD[3]. Remarkably, COPD has become the second leading cause of non-cancer deaths among individuals diagnosed with LC [4]. Repeated cycles of airway injury and repair associated with COPD create favorable conditions for cancer development[5].

Immunotherapy has revolutionized the treatment of LC, particularly non-small cell lung cancer (NSCLC). Several studies have demonstrated that NSCLC patients with COPD benefit more from immunotherapy compared to those without COPD, as indicated by prolonged survival rates and higher objective response rates (ORR)[6–9]. This therapeutic advantage may arise from alterations in the immune microenvironment induce by COPD[6,7]. Nevertheless, the precise biological mechanisms underlying the increased immunotherapy responsiveness in NSCLC patients with COPD remain poorly understood. Combined single-cell RNA sequencing (scRNA-seq) and spatial transcriptomics (ST-seq) provide a powerful approach to characterize immune cell populations and their interactions within the tumor microenvironment[10,11].

Understanding the complex relationship between COPD and NSCLC is crucial for improving treatment outcomes and prognosis for patients with coexistent conditions. Building upon this premise, our research employed scRNA-seq to identify the cellular heterogeneity specific to patients with NSCLC combined with COPD compared to those without COPD. These findings highlight how chronic inflammation shapes the tumor microenvironment, paving the way for future studies aimed at

understanding how COPD modulates immunotherapy efficacy in NSCLC. Additionally, our results provide a theoretical basis for the concurrent pharmacological management of NSCLC and COPD.

Results

COPD significantly impacts the immune environment of NSCLC

To investigate the cellular composition and gene regulation within the tumor microenvironment of NSCLC patients with (LC-COPD) and without COPD (LC-only), scRNA-seq was performed on 30 tumor samples (19 COPD, 11 non-COPD), 11 NAT samples (6 COPD, 5 non-COPD), and 23 peripheral blood samples (13 COPD, 10 non-COPD) (Figure 1A and Table S1). Following quality control, 534,996 high-quality cells with an average of 1,142 detected genes were identified, which underwent automated cell-type classification and marker-gene identification (Figure 1B–C and Figure S1A).

The abundance of immune cell subsets correlated with disease severity, as measured by the percent predicted forced expiratory volume in 1 second (FEV1), a key metric for evaluating lung function. Notably, increased monocyte fractions and decreased T-cell lineage populations correlated significantly with reduced FEV1%, indicating impaired lung function (Figure 1D–E and Figure S1B–G). Further analysis revealed lower proportions of T cells, macrophages, B cells and dendritic cells (DCs), but elevated monocyte fractions within tumors from patients with LC-COPD compared to those with LC-only. Conversely, NATs from LC-COPD cases displayed enriched T-cell populations (Figure 1F). Differentially expressed genes (DEG) analysis and pathway enrichment demonstrated distinct expression patterns and biological functions in malignant cells, DCs, and macrophages between the LC-COPD and LC-only groups (Figure 1G and Figure S1H). We found through cell interaction analysis that there are more interactions between immune cell subsets in LC-COPD, with macrophages showing the most prominent interactions with other cells (Figure S1I–J). Together, our scRNA-seq analysis highlights significant immune landscape heterogeneity and complexity associated with COPD in NSCLC.

Malignant cells in LC-COPD exhibit increased TGFβ1 expression and immune evasion

To characterize malignant cell composition and gene regulation differences in LC-only and LC-COPD, we analyzed tumor cells identified by clustering based on single-cell gene expression-derived copy number variations (CNVs) (Figure S2A–C). Malignant cells from 30 tumor samples clustered into 5 distinct subsets, each exhibiting specific enriched biological pathways (Figure 2A–B and Figure S2D). Pseudotime trajectory analysis indicated a progression of malignant cells toward distinct transcriptional states associated with immune evasion (Figure 2C–E). Malignant cells were in a state of immune evasion in LC-COPD, whereas they exhibited a state of immune surveillance in LC-only (Figure 2F–H). Specifically, transforming growth factor-beta 1 (TGFβ1)—a critical gene associated with immune escape mechanisms— showed heightened expression in LC-COPD cells, alongside reduced expression of HLA genes (Figure 2I–J), indicative of diminished immune recognition. Furthermore, increased TGFβ1

expression correlated with a decline in FEV1%, reflecting more severe disease (Figure 2K). These findings suggest that high TGFβ1 expression contributes to immune evasion in LC-COPD.

The transformation of normal epithelial cells to inflammatory epithelial cells and to malignant cells may be characterized by TGFβ1

The transformation of normal epithelial cells to inflammatory epithelial cells and ultimately to malignant cells is characterized by elevated TGFβ1 expression. In LC-COPD, normal epithelial cells already exhibit higher levels of TGFβ1 compared to LC-only cases (Figure 3A). This elevated TGFβ1 expression is also critical in driving the transition to malignant cells, where TGFβ1 levels are significantly higher than in the surrounding epithelial cells (Figure 3B). The elevated TGFβ1 expression not only drives the transformation from normal to malignant cells but also reduces immune surveillance and enhances immune escape in malignant cells, contributing to the formation of a tumor-immunosuppressive microenvironment (Figure 2C–E and Figure 3C). We then prepared cigarette smoke extract (CSE) (Figure 3D) and exposed A549 cells to CSE or lipopolysaccharide (LPS), noting a dose- and time-dependent increase in TGFβ1 expression (Figure 3E–H). Overall, these findings suggest that cigarette smoke and inflammation upregulate TGFβ1 in epithelial cells, contributing to progression from healthy lungs to COPD and eventually lung cancer (Figure 3I).

Exploring the role of TGFβ1 expression in malignant cells and its impact on macrophage subsets in LC-COPD

Given the marked upregulation of TGFβ1 in malignant epithelial cells in LC-COPD, we next asked whether this alteration reshapes the tumor immune microenvironment through enhanced crosstalk with immune cells. Cell–cell interaction analysis revealed that interactions between malignant cells and macrophages were markedly increased in LC-COPD compared with LC-only cases (Figure S2E), with macrophages emerging as a major cellular target of tumor-derived signals.To further assess how TGFβ1 expression in malignant cells influences macrophage populations, we classified macrophages into nine clusters, including four tumor-associated macrophage (TAM) clusters (Macro_IL4I1, Macro_MS4A6A, Macro_NEAT1, and Macro_VCAN) and five additional macrophage clusters (Macro_FABP4, Macro_IFI27, Macro_CCL4, Macro_STMN1, and Macro_HSPA1A) (Figure 4A–B and Figure S3A). Among these, Macro_IL4I1 predominated within tumor tissues, representing a distinct macrophage subset (Figure 4B).

We next sought to define macrophage subset characteristics through functional profiling. Traditionally, macrophages are categorized into M1 (proinflammatory or anti-tumor) and M2 (anti-inflammatory or pro-tumor) phenotypes. TAMs in LC-COPD exhibited a predominantly M2-like phenotype, whereas TAMs in LC-only samples displayed a stronger M1 signature (Figure S3B). Functional analyses further revealed that TAMs in LC-COPD showed enhanced angiogenic potential, while TAMs in LC-only demonstrated

superior phagocytic capacity and T-cell recruitment ability (Figure S3C). Notably, Macro_IL4I1, classified as an M2-like subset, contributed to both angiogenesis and inflammatory processes (Figure S3D–I). Analysis of TGFβ receptor–ligand interactions between malignant cells and Macro_IL4I1 or Macro_MS4A6A demonstrated a pronounced activation of TGFβ signaling in LC-COPD (Figure 4C). Spatial transcriptomic analysis further indicated that IL4I1 expression was predominantly localized to TAMs in LC-COPD tumors (Figure 4D–E).

Ligand–receptor interaction analysis revealed more extensive crosstalk between macrophages and other immune cell populations in LC-COPD, with the most prominently upregulated interaction involving LGALS9 and its receptors between macrophages and $CD8^+$ T cells (Figure 4F). Consistently, we observed that TGFβ1 stimulation promoted IL4I1 expression and activated TGFβ signaling in macrophages in a dose/time-dependent manner (Figure 4G–H). Moreover, using western blotting, qPCR, and ELISA assays, we found that TGFβ1 stimulation significantly induced LGALS9 expression in macrophages (Figure 4H–J). Spatial transcriptomic analysis further revealed elevated IL4I1 expression in regions where TAMs and $CD8^+$ T cells were colocalized, suggesting that $IL4I1^+$ macrophages may play a critical role in mediating macrophage–$CD8^+$ T-cell interactions (Figure 4K).

In conclusion, our study highlights a pivotal role for malignant cell–derived TGFβ1 in shaping the LC-COPD tumor immune microenvironment by promoting the expansion and functional activation of $IL4I1^+$ macrophages and enhancing their LGALS9-mediated immunomodulatory effects.

Immunosuppressive phenotypes of T cells in LC-COPD

We next investigated whether the TGFβ1–$IL4I1^+$ TAM–LGALS9 axis in LC-COPD is associated with T-cell dysfunction in the tumor microenvironment. T cells play a crucial role in the effectiveness of current cancer immunotherapies[12]. To profile T lymphocytes at higher resolution, we subclustered them into 10 annotated $CD4^+$ subsets—interferon-stimulated genes (ISG)–positive T cells, effector memory T cells (Tem), terminally differentiated effector memory or effector cells (Temra), follicular helper T cells (Tfh), Tfh/T helper 1 cells (TfhTh1), T helper cells 17 (Th17), memory T cells (Tm), naive T cells (Tn), regulatory T cells (Treg) and mixed T cells (Tmix). Additionally, 9 $CD8^+$ T-cell clusters were identified, including ISG^+ T cells, mucosal-associated invariant T cells (MAIT), Tem, Temra, exhausted $CD8^+$ T cells (Tex), NK-like T cells (Tk), Tm, Tn, and tissue-resident memory T cells (Trm) (Figure 5A and Figure S4A–B).

We observed that the proportions of CD4_Treg and CD4_Tm were significantly higher in LC-COPD than in LC-only for both adenocarcinoma and squamous carcinoma (Figure 5B). In parallel, the proportion of CD8_Tex was markedly elevated in LC-COPD across both NSCLC subtypes (Figure 5C). These CD8_Tex cells exhibited a strong exhaustion signature, particularly in LC-COPD (Figure 5D). Flow cytometry further confirmed an increased frequency of $PD1^+$ and $TIGIT^+$ subpopulations within $CD8^+$ T cells from patients with LC-COPD (Figure 5E–F and Figure S5A).

Because tumor-specific T cells are essential for anti-tumor immunity[13-15], we evaluated their tumor specificity score[16] and found it to be notably higher in exhausted T-cell subsets, especially in LC-COPD (Figure S4C–D). Using a TCR-based approach that identified shared clonotypes with Tex cells and high tumor-specific T-cell gene expression scores (>0), we isolated a population of $CD8^+$ tumor-specific T cells characterized by distinct clonotypes (Figure S4E–G). This tumor-specific subset was more abundant in LC-COPD (Figure 5G). Compared with unrelated T cells, LGALS9 displayed stronger interactions with these tumor-associated T cells, and this effect was more pronounced in LC-COPD (Figure 5H). Notably, among tumor-associated macrophage subsets, LGALS9–receptor interactions with tumor-specific $CD8^+$ T cells were most prominent in the Macro_IL4I1 and Macro_MS4A6A populations in LC-COPD (Figure 5H).

CXCL13 and CD82 serve as markers for exhausted, tumor-specific $CD8^+$ T Cells associated with favorable prognosis.

Based on marker genes and functional scores, we identified nine distinct tumor-specific $CD8^+$ T-cell subtypes: CD8_Temra_GZMH, CD8_Tex_RGS1, CD8_Trm_ZNF683, CD8_Tem_GZMK, CD8_progenitor exhausted cluster_IL7R (CD8_pTex_IL7R), CD8_Tex_GZMB, CD8_proliferative_STMN1 (CD8_Tpro_STMN1), CD8_Trm_CXCR4, and CD8_Treg_FOXP3 (Figure 6A and Figure S6A). Classification accuracy for these subsets was validated by mapping them back to their original $CD8^+$ T-cell clusters (Figure S6B).

Of these, CD8_Tex_RGS1 and CD8_Tex_GZMB showed high exhaustion scores, with only the CD8_Tex_GZMB subset exhibiting strong cytotoxicity (Figure 6B). All CD8_Tex and CD8_pTex subsets were enriched in cytokine-cytokine receptor interaction pathway. Additionally, CD8_Tex_GZMB, CD8_Tex_RGS1, and CD8_pTex_IL7R were particularly abundant in IL10, TNF, and STAT signaling pathways, respectively (Figure S6C). Chemokine C-X-C motif ligand 13 (CXCL13) and CD82 emerged as shared top markers for both the CD8_Tex_GZMB and CD8_Tex_RGS1 clusters (Figure 6C). Moreover, significantly more tumor-specific $CD8^+$ T cells co-expressed these genes compared with tumor-unrelated $CD8^+$ T cells (Figure 6D). CXCL13 and CD82 were also expressed at higher levels in LC-COPD tumors than in NATs (Figure S6D). Consistent with their potential clinical relevance, TCGA data indicated that higher expression of both markers correlated with better PFS in patients with NSCLC (Figure 6E–F).

Tumor-specific $CD8^+$ T cells reside in an exhausted state in LC-COPD and a cytotoxic state in LC-only

Building on the identification of CXCL13 and CD82 as markers of tumor-specific $CD8^+$ T cells with favorable prognostic significance, we next investigated their developmental origins and state transitions. TCR analyses suggested that the two CD8_Tex subsets primarily originate from the CD8_Tpro_STMN1 cluster (Figure 6G). While CD8_Temra_GZMH, CD8_Trm_ZNF683, and CD8_Tem_GZMK were more

abundant in LC-only, exhaustion-related clusters (CD8_pTex_IL7R, CD8_Tex_RGS1 and CD8_Tex_GZMB) prevailed in LC-COPD (Figure 6H). We inferred state trajectories and examined dynamic cell transitions to illustrate the distinctive immunological states of tumor specific $CD8^+$ T cells in LC-COPD versus LC-only (Figure 6I). As cells progressed along this trajectory, cytotoxic signatures increased, while the exhaustion score reached its maximum at the fully exhausted state (Figure S6E). Pseudotime trajectory analyses positioned CD8_Tpro_STMN1 at the earliest differentiation stage (in the absence of naive T cells) and identified CD8_Tex and CD8_Temra_GZMH as terminally differentiated states (Figure 6J). Some CD8_Tex cells originated directly from CD8_Tpro_STMN1, whereas others transitioned from CD8_Tpro_STMN1 via an intermediate state involving CD8_Trm_ZNF683, CD8_Treg_FOXP3, and CD8_pTex_IL7R (Figure 6J). Additionally, the intermediate state could also transition to an effector memory state characterized by CD8_Tem_GZMK and CD8_Temra_GZMH (Figure 6J).

In LC-COPD, the initial or intermediate state showed a higher propensity to transition into an exhausted $CD8^+$ T cell state (Figure 6K). By contrast, the intermediate state in LC-only followed two distinct trajectories, one leading to exhaustion and the other toward a cytotoxic effector memory state (Figure 6L). CXCL13 and CD82 expression were elevated in both the initial proliferative and exhausted states (Figure 6L). Correlation analysis further indicated a positive association between CXCL13/CD82 expression and T-cell exhaustion (Figure S6F). Consistently, Gal-9 stimulation promoted CXCL13 and CD82 expression in $CD8^+$ T cells in a dose-dependent manner (Figure 6M). Given that proliferative tumor-specific $CD8^+$ T cells are considered a key reservoir sustaining effective anti-tumor immunity, these findings suggest that Gal-9 signaling may facilitate the expansion or maintenance of such proliferative $CD8^+$ T-cell populations through the induction of CXCL13 and CD82.

Overall, our analysis reveals distinct immune and transcriptional states during tumor-specific $CD8^+$ T-cell differentiation in LC-COPD. Rather than serving solely as markers of exhaustion, CXCL13 and CD82 identify tumor-specific $CD8^+$ T cells with enhanced proliferative potential. Together with the observed enrichment of these populations in LC-COPD and their association with improved patient outcomes, our findings support a model in which TGFβ-driven $IL4I1^+$ macrophages shape tumor-specific $CD8^+$ T-cell states through Gal-9 signaling, thereby influencing the balance between proliferation and exhaustion.

Discussion

Immunotherapy has become a cornerstone of NSCLC treatment[17]. Patients' preexisting immune status significantly affects the efficacy of these therapies[18]. COPD, a common comorbidity in lung cancer, profoundly reshapes pulmonary immunity; however, how COPD alters the tumor immune microenvironment and influences immune escape mechanisms in lung cancer remains incompletely understood. In this study, we performed an integrated single-cell and spatial transcriptomic analysis of treatment-naïve NSCLC tissues to systematically compare the immune ecosystems of LC-COPD and LC-only.

Our findings indicate that LC-COPD and LC-only tumors employ different immune escape mechanisms. TGF-β, a key regulator of tumor progression and immune suppression[19], was markedly upregulated in LC-COPD. This finding is consistent with prior reports implicating aberrant TGF-β signaling in both COPD and lung cancer[20,21] and supports the notion that chronic airway inflammation may facilitate malignant transformation through sustained TGF-β activation[22]. Dysregulated TGF-β signaling correlates with therapy resistance in lung cancer[19], consistent with clinical observations that patients with LC-COPD display greater resistant to anti-tumor drugs. We observed that LC-COPD tumor cells express higher levels of TGFβ1 and exhibit more frequent TGFβ-mediated crosstalk with DCs and TAMs, thus contributing to an immunosuppressive microenvironment. Although various TGF-β inhibitors are in clinical or preclinical trials[19,23,24], their combination with PD-1/PD-L1 blockers has shown limited success, possibly due to inadequate patient selection or trial design[25]. Targeting TGF-β in LC-COPD may identify patients who benefit most and guide more effective combination therapies.

A particularly notable feature of the LC-COPD tumor microenvironment is the expansion of IL4I1-expressing tumor-associated macrophages. IL4I1 (interleukin-4–induced gene 1) encodes an L-amino acid oxidase originally characterized in antigen-presenting cells and has been implicated in immune regulation through metabolic and redox-dependent mechanisms[26]. Previous studies have shown that IL4I1 can suppress T-cell proliferation and effector function by depleting essential amino acids and generating immunoregulatory metabolites, thereby contributing to immune tolerance in both inflammatory and tumor contexts[27]. In cancer, IL4I1 expression has been reported in myeloid populations and linked to poor prognosis and immune evasion, although its precise role within distinct macrophage subsets remains incompletely defined.

In the context of LC-COPD, the enrichment of IL4I1$^+$ TAMs suggests that chronic inflammatory cues and tumor-derived signals converge to promote a specialized immunomodulatory macrophage phenotype. Sustained TGFβ signaling, which is prominent in COPD-associated lung cancer, may favor the differentiation or stabilization of IL4I1$^+$ macrophages, thereby reinforcing local immune suppression. Rather than acting solely as passive inhibitors of immunity, these macrophages appear positioned to actively shape the tumor immune ecosystem by orchestrating intercellular communication networks.

One potential mechanism through which IL4I1$^+$ TAMs influence tumor immunity is via the regulation of Gal-9–mediated signaling. Gal-9 has been widely recognized as an immunomodulatory ligand capable of altering T-cell activation, differentiation, and survival in a context-dependent manner[28–30]. While Gal-9 has often been associated with inhibitory effects on T cells, emerging evidence suggests that its impact may vary depending on the differentiation state of T cells and the broader cytokine milieu[31]. In LC-COPD tumors, IL4I1$^+$ macrophages may serve as a major source of Gal-9, thereby modulating tumor-specific CD8$^+$ T-cell programs rather than inducing uniform terminal dysfunction.

Importantly, this macrophage-driven signaling landscape may help reconcile the apparent paradox observed in LC-COPD tumors, which exhibit features of immune suppression alongside the preservation

of tumor-specific CD8⁺ T-cell populations with proliferative capacity. By influencing the balance between T-cell proliferation and differentiation, IL4I1⁺ TAMs could contribute to maintaining a reservoir of tumor-reactive CD8⁺ T cells poised for reactivation upon immune checkpoint blockade. Such a model aligns with emerging concepts that effective immunotherapy responses rely not on the complete absence of inhibitory signals, but on the presence of a sufficiently large and dynamic pool of tumor-specific T cells capable of functional reinvigoration.

Our study also revealed distinct immune profiles of $CD8^+$ T cells, especially in the presence of COPD. Patients with LC-COPD had $CD8^+$ T cells with both heightened tumor specificity and stronger exhaustion compared to LC-only. This aligns with prior findings that the degree of T-cell exhaustion parallels tumor specificity[32]. Some research suggests that PD-L1 expression in tumors predicts the presence of tumor-reactive $CD8^+$ T cells[12], which may help explain improved responses to anti-PD-1/PD-L1 therapy in LC-COPD[33]. Efforts to define precursor exhausted T cells with stem-like properties have identified potential biomarkers of immunotherapy response[34–36]. Our data, integrating TCR and trajectory data, show that most CD8_Tex cells arise directly from a proliferative CD8_Tpro_STMN1 subset. While typical exhaustion markers such as TCF7 and IL7R did not fully characterize CD8_Tpro_STMN1, both CXCL13 and CD82—associated with T-cell dysfunction and immune therapy response—were highly expressed in this population. CXCL13 has been recognized as a marker for T-cell dysfunction and tumor antigen specificity, as well as a predictive biomarker for immunotherapy across various tumor types[37–41]. Moreover, $CD8^+$ T cells expressing CXCL13 are considered to be proliferative[39]. Consistent with this notion, we observed elevated CXCL13 and CD82 expression in proliferative CD8⁺ T-cell subsets and demonstrated that Gal-9 stimulation—derived predominantly from IL4I1⁺ TAMs—induced CXCL13 and CD82 expression in a dose-dependent manner. These findings suggest that Gal-9 signaling may promote the expansion or maintenance of tumor-specific, proliferative CD8⁺ T cells, rather than solely driving terminal exhaustion.

In summary, our study delineates a distinct immune architecture in LC-COPD characterized by TGFβ1-driven malignant–myeloid interactions, expansion of IL4I1⁺ TAMs, and remodeling of tumor-specific CD8⁺ T-cell differentiation trajectories. Rather than representing a uniformly immune-excluded state, LC-COPD tumors harbor a complex immune ecosystem in which immunosuppressive signals coexist with proliferative tumor-specific T-cell populations. These insights deepen our understanding of immune regulation in LC-COPD and highlight IL4I1⁺ TAMs and their downstream signaling pathways as potential modulators of immunotherapy responsiveness. Collectively, our findings provide a conceptual framework for refining patient stratification and developing tailored immunotherapeutic strategies for NSCLC patients with COPD.

Methods

Sample Collection and Cell Preparation

Fresh lung tumor tissues and peripheral blood samples were collected from patients following ethical approval (K2022179) from The Fourth Affiliated Hospital of Zhejiang University School of Medicine and The Second Affiliated Hospital Zhejiang University School of Medicine. Informed consent was obtained from all participants. Tissue samples were mechanically dissociated and enzymatically digested to obtain single-cell suspensions. Peripheral blood mononuclear cells (PBMCs) were isolated using density gradient centrifugation. Cell viability was assessed using trypan blue staining. The clinical and pathological characteristics of the patients are listed in Table S1.

Single-cell RNA Sequencing

Single-cell suspensions were loaded onto microfluidic devices and processed using the Singleron GEXSCOPE® Single-Cell RNA Library Kit. Libraries were sequenced on an Illumina NovaSeq 6000 platform (150 bp paired-end reads). Raw sequencing data were processed with quality control, doublet detection, and batch effect correction using Scanpy, scDblFinder, SoupX, and Harmony.

Data Analysis and Clustering

Normalized and log-transformed expression matrices were subjected to principal component analysis (PCA) for dimensionality reduction, followed by UMAP visualization and Leiden clustering. Differentially expressed genes (DEGs) were identified using t-tests with false discovery rate correction (FDR < 0.05).

Cell Type Annotation and Malignancy Inference

Clusters were annotated using the Human Leukocyte Cell Atlas reference and scANVI transfer learning for fine T cell subtyping. Putative malignant cells were identified via inferred copy number variation (CNV) from scRNA-seq data using smoothed chromosomal expression patterns.

Functional and Pathway Analysis

Gene set enrichment analysis (GSEA) and overrepresentation analysis (Enrichr) were used to identify biological pathways associated with cluster-specific signatures. Functional scores for pathways or signatures were calculated per cell using a reference-based z-score approach. All signatures were got from previous studies (Table S2-4).

Spatial Transcriptomics

Spatial gene expression profiles were obtained using the 10× Genomics Visium platform. Cell-type deconvolution was performed with cell2location using annotated single-cell RNA-seq references, producing spot-wise cell-type abundance maps.

In vitro Cell Assays

A549 and THP1 cells, and isolated human $CD8^+$ T cells, were cultured under standard conditions. Cells were stimulated with cytokines, cigarette smoke extract (CSE), lipopolysaccharide (LPS), or recombinant proteins for functional assays. Protein expression was assessed by Western blot, RNA levels by quantitative RT-PCR, and secreted factors by ELISA. The primers are shown in Table S5.

Survival and Clinical Correlation Analysis

Gene signatures were correlated with overall or progression-free survival in TCGA lung cancer cohorts using Kaplan-Meier analysis and log-rank testing. Correlations between cell-type proportions and lung function metrics (FEV1%, FEV1/FVC) were assessed using Pearson correlation after appropriate transformation.

Statistical Analysis

Comparisons between groups were performed using non-parametric tests (Mann–Whitney U or Kruskal–Wallis H tests), with multiple hypothesis testing controlled via the Benjamini–Hochberg procedure (adjusted $p < 0.05$ considered significant).

Detailed experimental procedures, reagents, and protocols are provided in the Supplementary Methods.

Declarations

Competing interests

The authors declare no competing interests.

Author Contribution

MX conceived the study design, performed experiments, acquired and processed the cohort data, conceptualized and implemented data analysis, and wrote the manuscript with GC and YX designed, performed, and analyzed all flow cytometry experiments. XZ and YC assisted with spatial transcriptomic data analysis. YG, YYand MZ carried out the patient phenotyping. JZ, KW and ZZ supervised the work.

Acknowledgement

This work is supported by the National Natural Science Foundation of China (U23A20467), National Key R&D Program of China (2024YFA1108500), the National Natural Science Foundation of China (No.

82102852) and Science and Technology program of Jinhua Science and Technology Bureau (Grant No.2023-3-058). We would like to acknowledge the Biobank staff of Second Affiliated Hospital of Zhejiang University and the staff in the departments of respiratory and thoracic surgery in The Fourth Affiliated Hospital of Zhejiang University School of Medicine for their hard work and dedication to our investigators for their support and to the study participants.We would like to thank Editage (www.editage.cn) for English language editing.

Data availability

The processed expression data of SC and ST reported in this study can be obtained from the China National GeneBank Database (CNGBdb) with accession number (GSA: HRA010788, HRA010787, HRA010890). This paper does not report original code.

References

1. Celli, B. R. & Wedzicha, J. A. Update on Clinical Aspects of Chronic Obstructive Pulmonary Disease. *N Engl J Med* **381**, 1257-1266, doi:10.1056/NEJMra1900500 (2019).
2. Wang, C. *et al.* Prevalence and risk factors of chronic obstructive pulmonary disease in China (the China Pulmonary Health [CPH] study): a national cross-sectional study. *Lancet* **391**, 1706-1717, doi:10.1016/s0140-6736(18)30841-9 (2018).
3. Carr, L. L. *et al.* Features of COPD as Predictors of Lung Cancer. *Chest* **153**, 1326-1335, doi:10.1016/j.chest.2018.01.049 (2018).
4. Zheng, Y. *et al.* Deaths from COPD in patients with cancer: a population-based study. *Aging (Albany NY)* **13**, 12641-12659, doi:10.18632/aging.202939 (2021).
5. Shin, J. I. & Brusselle, G. G. Mechanistic links between COPD and lung cancer: a role of microRNA let-7? *Nat Rev Cancer* **14**, 70, doi:10.1038/nrc3477-c1 (2014).
6. Mark, N. M. *et al.* Chronic Obstructive Pulmonary Disease Alters Immune Cell Composition and Immune Checkpoint Inhibitor Efficacy in Non-Small Cell Lung Cancer. *Am J Respir Crit Care Med* **197**, 325-336, doi:10.1164/rccm.201704-0795OC (2018).
7. Biton, J. *et al.* Impaired Tumor-Infiltrating T Cells in Patients with Chronic Obstructive Pulmonary Disease Impact Lung Cancer Response to PD-1 Blockade. *Am J Respir Crit Care Med* **198**, 928-940, doi:10.1164/rccm.201706-1110OC (2018).
8. Shin, S. H. *et al.* Improved treatment outcome of pembrolizumab in patients with nonsmall cell lung cancer and chronic obstructive pulmonary disease. *Int J Cancer* **145**, 2433-2439, doi:10.1002/ijc.32235 (2019).
9. Zhou, J. *et al.* Impact of chronic obstructive pulmonary disease on immune checkpoint inhibitor efficacy in advanced lung cancer and the potential prognostic factors. *Transl Lung Cancer Res* **10**,

2148-2162, doi:10.21037/tlcr-21-214 (2021).

10. Gueguen, P. *et al.* Contribution of resident and circulating precursors to tumor-infiltrating CD8(+) T cell populations in lung cancer. *Sci Immunol* **6**, doi:10.1126/sciimmunol.abd5778 (2021).
11. Wang, Y. *et al.* Spatial transcriptomics delineates molecular features and cellular plasticity in lung adenocarcinoma progression. *Cell Discov* **9**, 96, doi:10.1038/s41421-023-00591-7 (2023).
12. Chow, A., Perica, K., Klebanoff, C. A. & Wolchok, J. D. Clinical implications of T cell exhaustion for cancer immunotherapy. *Nat Rev Clin Oncol* **19**, 775-790, doi:10.1038/s41571-022-00689-z (2022).
13. Jansen, C. S. *et al.* An intra-tumoral niche maintains and differentiates stem-like CD8 T cells. *Nature* **576**, 465-470, doi:10.1038/s41586-019-1836-5 (2019).
14. Luoma, A. M. *et al.* Tissue-resident memory and circulating T cells are early responders to pre-surgical cancer immunotherapy. *Cell* **185**, 2918-2935.e2929, doi:10.1016/j.cell.2022.06.018 (2022).
15. Oliveira, G. & Wu, C. J. Dynamics and specificities of T cells in cancer immunotherapy. *Nat Rev Cancer* **23**, 295-316, doi:10.1038/s41568-023-00560-y (2023).
16. Chen, S. *et al.* Distinct single-cell immune ecosystems distinguish true and de novo HBV-related hepatocellular carcinoma recurrences. *Gut* **72**, 1196-1210, doi:10.1136/gutjnl-2022-328428 (2023).
17. Reck, M., Remon, J. & Hellmann, M. D. First-Line Immunotherapy for Non-Small-Cell Lung Cancer. *J Clin Oncol* **40**, 586-597, doi:10.1200/jco.21.01497 (2022).
18. Hu, J. *et al.* Tumor microenvironment remodeling after neoadjuvant immunotherapy in non-small cell lung cancer revealed by single-cell RNA sequencing. *Genome Med* **15**, 14, doi:10.1186/s13073-023-01164-9 (2023).
19. Derynck, R., Turley, S. J. & Akhurst, R. J. TGFβ biology in cancer progression and immunotherapy. *Nat Rev Clin Oncol* **18**, 9-34, doi:10.1038/s41571-020-0403-1 (2021).
20. Ghosh, A. J. *et al.* Lung tissue shows divergent gene expression between chronic obstructive pulmonary disease and idiopathic pulmonary fibrosis. *Respir Res* **23**, 97, doi:10.1186/s12931-022-02013-w (2022).
21. Wang, B., Zhang, Z., Tang, J., Tao, H. & Zhang, Z. Correlation between SPARC, TGFβ1, Endoglin and angiogenesis mechanism in lung cancer. *J Biol Regul Homeost Agents* **32**, 1525-1531 (2018).
22. Wang, D. C., Shi, L., Zhu, Z., Gao, D. & Zhang, Y. Genomic mechanisms of transformation from chronic obstructive pulmonary disease to lung cancer. *Semin Cancer Biol* **42**, 52-59, doi:10.1016/j.semcancer.2016.11.001 (2017).
23. Massagué, J. & Sheppard, D. TGF-β signaling in health and disease. *Cell* **186**, 4007-4037, doi:10.1016/j.cell.2023.07.036 (2023).
24. Kim, B. G., Malek, E., Choi, S. H., Ignatz-Hoover, J. J. & Driscoll, J. J. Novel therapies emerging in oncology to target the TGF-β pathway. *J Hematol Oncol* **14**, 55, doi:10.1186/s13045-021-01053-x (2021).
25. Metropulos, A. E., Munshi, H. G. & Principe, D. R. The difficulty in translating the preclinical success of combined TGFβ and immune checkpoint inhibition to clinical trial. *EBioMedicine* **86**, 104380,

doi:10.1016/j.ebiom.2022.104380 (2022).

26. Mazzoni, A. *et al.* IL4I1 Is Expressed by Head-Neck Cancer-Derived Mesenchymal Stromal Cells and Contributes to Suppress T Cell Proliferation. *J Clin Med* **10**, doi:10.3390/jcm10102111 (2021).
27. Lasoudris, F. *et al.* IL4I1: an inhibitor of the CD8⁺ antitumor T-cell response in vivo. *Eur J Immunol* **41**, 1629-1638, doi:10.1002/eji.201041119 (2011).
28. An, G. *et al.* Osteoclasts promote immune suppressive microenvironment in multiple myeloma: therapeutic implication. *Blood* **128**, 1590-1603, doi:10.1182/blood-2016-03-707547 (2016).
29. Chretien, A. S. *et al.* Natural Killer Defective Maturation Is Associated with Adverse Clinical Outcome in Patients with Acute Myeloid Leukemia. *Front Immunol* **8**, 573, doi:10.3389/fimmu.2017.00573 (2017).
30. Arias-Pinilla, G. A. & Modjtahedi, H. Therapeutic Application of Monoclonal Antibodies in Pancreatic Cancer: Advances, Challenges and Future Opportunities. *Cancers (Basel)* **13**, doi:10.3390/cancers13081781 (2021).
31. Valero-Martínez, C. *et al.* Differential Expression of Galectin-1 and Galectin-9 in Immune-Mediated Inflammatory Diseases. *Int J Mol Sci* **26**, doi:10.3390/ijms26189087 (2025).
32. Thommen, D. S. *et al.* A transcriptionally and functionally distinct PD-1(+) CD8(+) T cell pool with predictive potential in non-small-cell lung cancer treated with PD-1 blockade. *Nat Med* **24**, 994-1004, doi:10.1038/s41591-018-0057-z (2018).
33. Lin, M., Huang, Z., Chen, Y., Xiao, H. & Wang, T. Lung cancer patients with chronic obstructive pulmonary disease benefit from anti-PD-1/PD-L1 therapy. *Front Immunol* **13**, 1038715, doi:10.3389/fimmu.2022.1038715 (2022).
34. Gettinger, S. N. *et al.* A dormant TIL phenotype defines non-small cell lung carcinomas sensitive to immune checkpoint blockers. *Nat Commun* **9**, 3196, doi:10.1038/s41467-018-05032-8 (2018).
35. Brummelman, J. *et al.* High-dimensional single cell analysis identifies stem-like cytotoxic CD8(+) T cells infiltrating human tumors. *J Exp Med* **215**, 2520-2535, doi:10.1084/jem.20180684 (2018).
36. Im, S. J. *et al.* Defining CD8+ T cells that provide the proliferative burst after PD-1 therapy. *Nature* **537**, 417-421, doi:10.1038/nature19330 (2016).
37. Liu, B. *et al.* Temporal single-cell tracing reveals clonal revival and expansion of precursor exhausted T cells during anti-PD-1 therapy in lung cancer. *Nat Cancer* **3**, 108-121, doi:10.1038/s43018-021-00292-8 (2022).
38. Liu, B., Zhang, Y., Wang, D., Hu, X. & Zhang, Z. Single-cell meta-analyses reveal responses of tumor-reactive CXCL13(+) T cells to immune-checkpoint blockade. *Nat Cancer* **3**, 1123-1136, doi:10.1038/s43018-022-00433-7 (2022).
39. Dai, S. *et al.* Intratumoral CXCL13(+)CD8(+)T cell infiltration determines poor clinical outcomes and immunoevasive contexture in patients with clear cell renal cell carcinoma. *J Immunother Cancer* **9**, doi:10.1136/jitc-2020-001823 (2021).

40. Pichler, R. *et al.* A chemokine network of T cell exhaustion and metabolic reprogramming in renal cell carcinoma. *Front Immunol* **14**, 1095195, doi:10.3389/fimmu.2023.1095195 (2023).
41. Wischnewski, V. *et al.* Phenotypic diversity of T cells in human primary and metastatic brain tumors revealed by multiomic interrogation. *Nat Cancer* **4**, 908-924, doi:10.1038/s43018-023-00566-3 (2023).

Figures

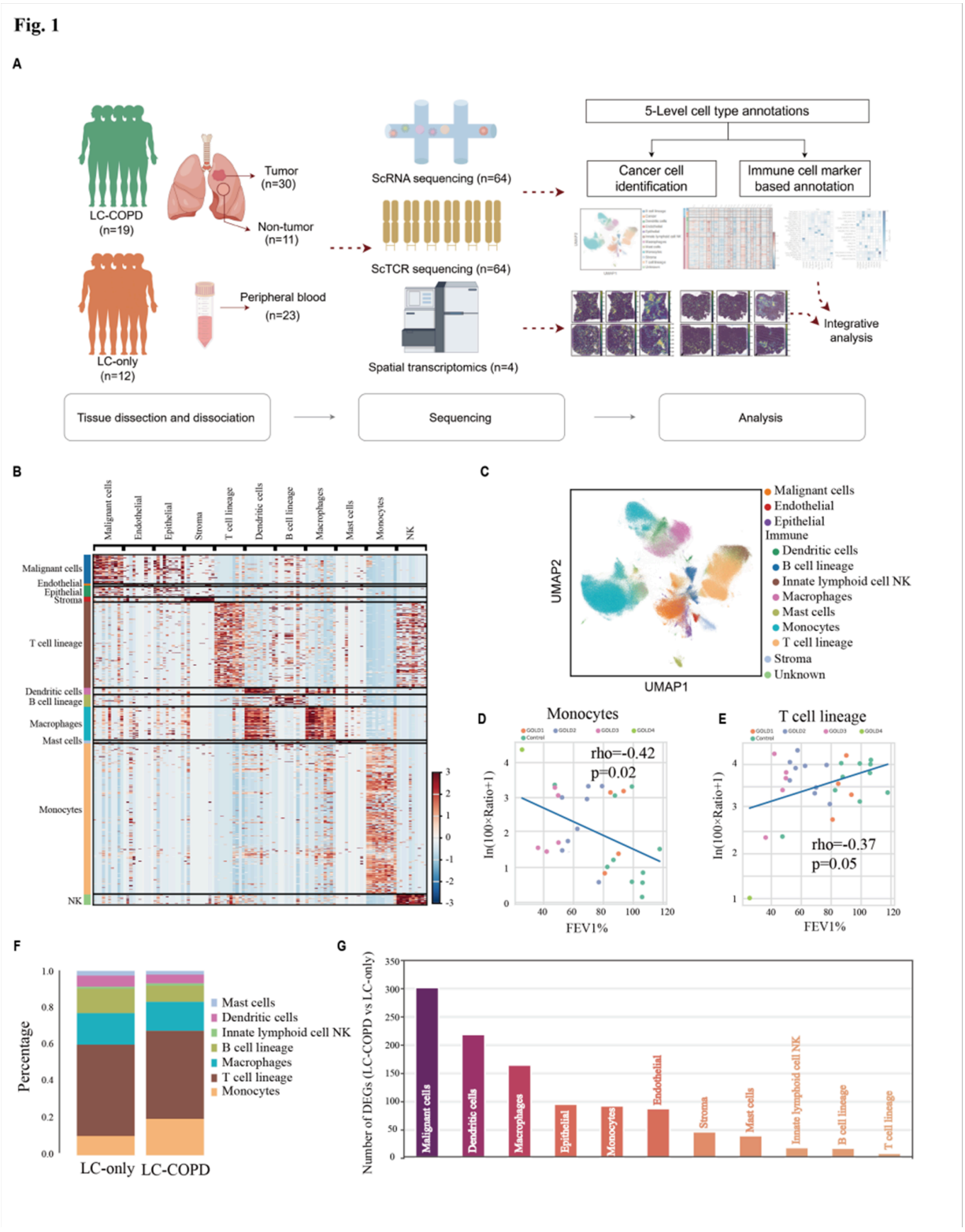


Figure 1

Lung cancer immune ecosystem characterized by single-cell transcriptomic sequencing in patients with and without chronic obstructive pulmonary disease (COPD).

(A) Schematic overview of the study design.

(B) Heatmap showing marker gene expression across identified cell types.

(C) Uniform manifold approximation and projection (UMAP) visualization of cell clusters.

(D–E) Correlation of immune cell subset abundance with lung function severity, measured by percentage forced expiratory volume in 1 s (FEV1%). Disease severity classified according to Global Initiative for Chronic Obstructive Lung Disease (GOLD) guidelines.

(F) Comparison of cell fractions in tumor tissues between NSCLC patients with (LC-COPD) and without COPD (LC-only).

(G) Number of differentially expressed genes (DEGs) identified in major cell subsets comparing NSCLC with and without COPD.

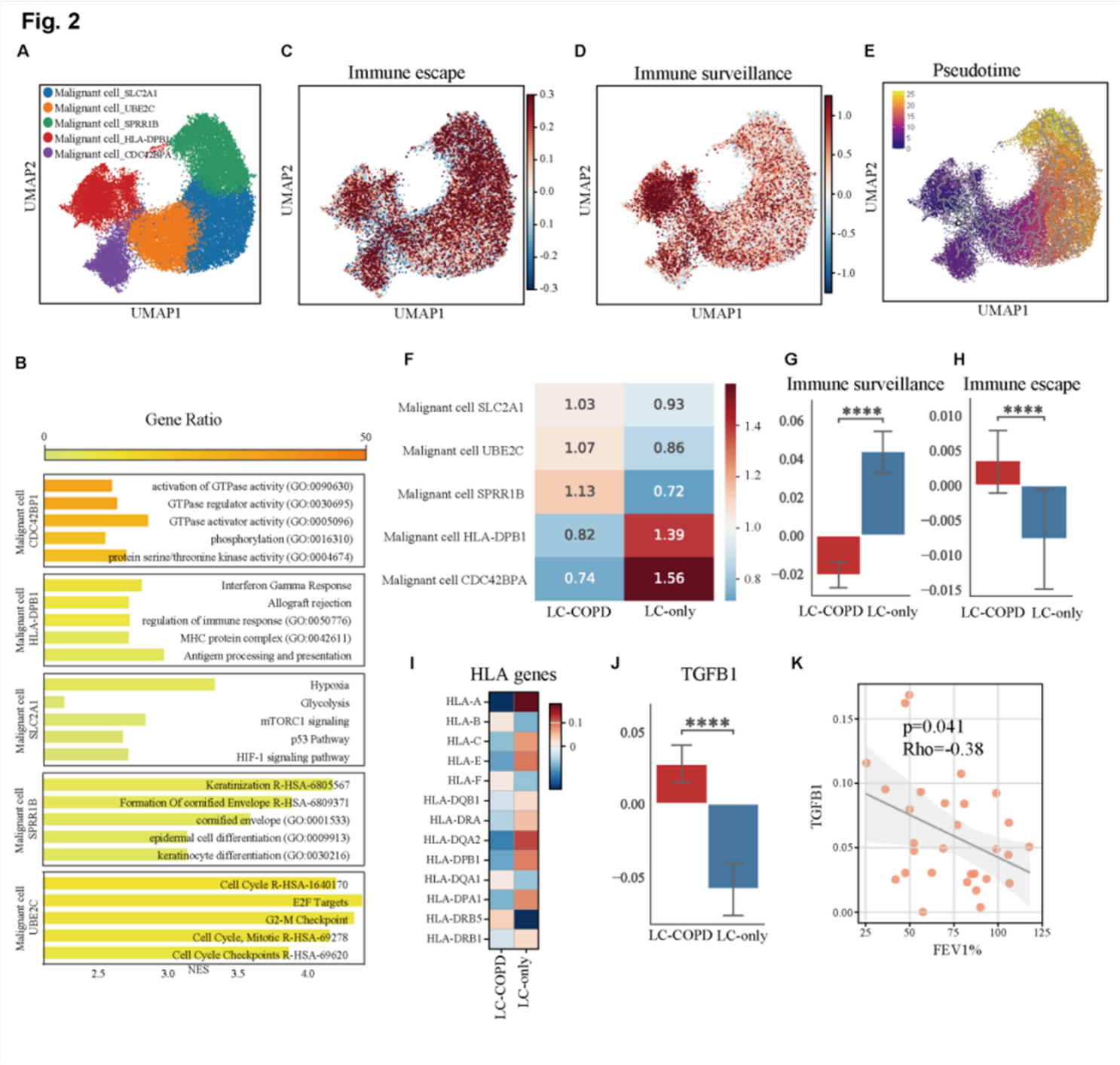


Figure 2

Immune suppression of malignant cells correlates with COPD.

(A) UMAP plot depicting five clusters of malignant cells.

(B) Gene set enrichment analysis of cluster-specific markers using MSigDB, GO and KEGG databases.

(C–D) UMAP plots showing expression of immune escape and immune surveillance markers.

(E) Pseudotime trajectory of malignant cells.

(F) Heatmap indicating the relative enrichment of malignant cells in the tumor microenvironment for NSCLC with and without COPD.

(G–H) Boxplots of normalized immune escape and immune surveillance scores in malignant cells from LC-COPD and LC-only.

(I) Expression patterns of HLA genes in malignant cell subsets.

(J) Boxplot comparing TGFβ1 expression between LC-COPD and LC-only.

(K) Correlation analysis between TGFβ1 expression in malignant cells and FEV1%.

*p < 0.05, **p < 0.01, ***p < 0.001, ****p < 0.0001.

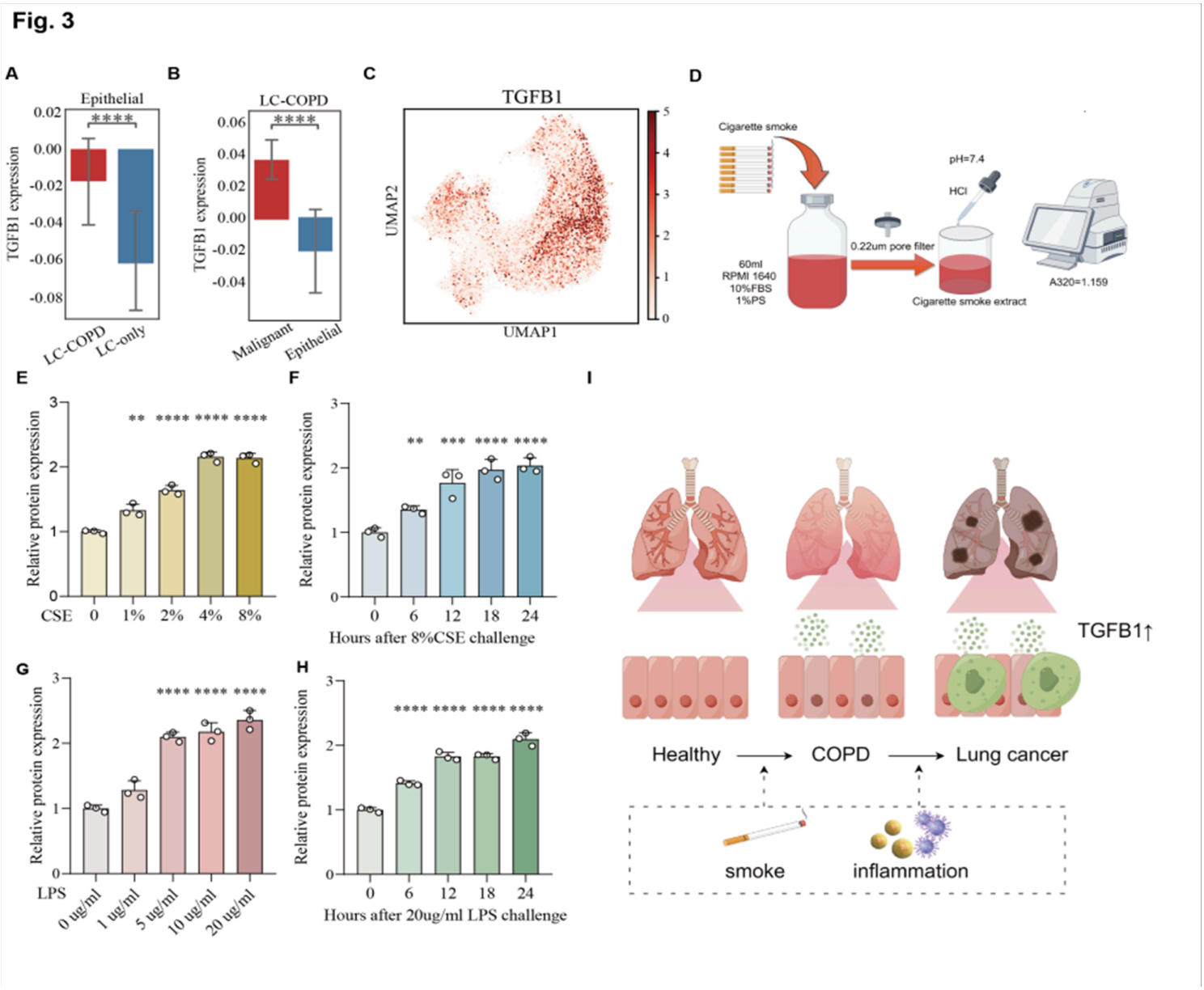


Figure 3

TGFβ1 expression elevation during malignant transformation of epithelial cells in NSCLC with COPD.

(A) Boxplot of TGFβ1 expression of epithelial cells in NSCLC-COPD and NSCLC-only.

(B) Boxplot of TGFβ1 expression of malignant cells and epithelial cells in NSCLC-COPD.

(C) UMAP plots showing expression of TGFβ1.

(D) Schematics of the extraction procedure by Figdraw.

(E-H) Histogram of TGFβ1 expression levels in A549 cells treated with LPS and CSE at different concentrations and times.

(I) Diagram summarizing the expression of TGFβ1 increased during malignant transformation of epithelial cells in LC-COPD by Figdraw.

* $p < 0.05$, ** $p < 0.01$, *** $p < 0.001$, **** $p < 0.0001$.

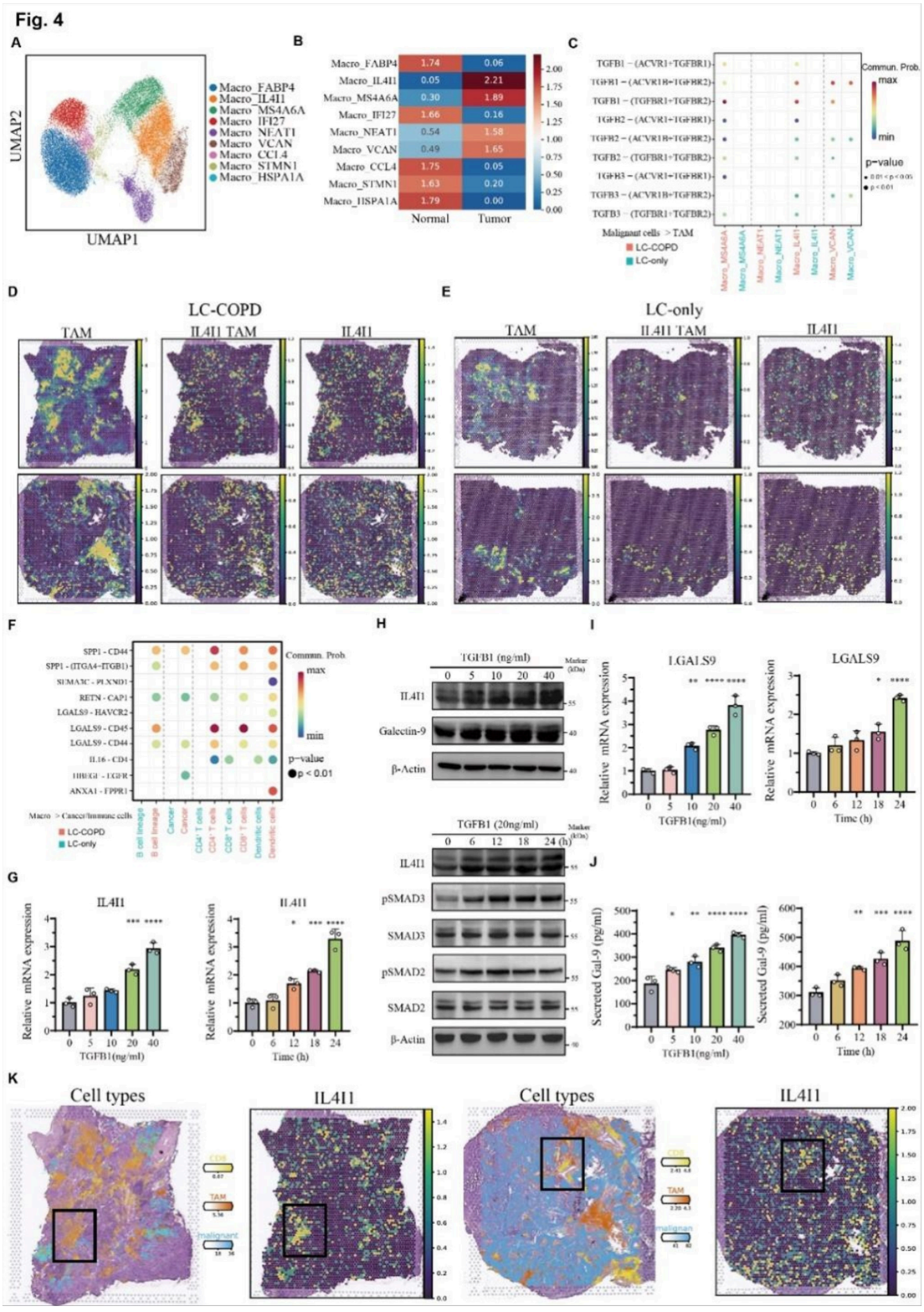


Figure 4

TGFβ1-IL4I1-mediated interactions and their impact on the tumor microenvironment of LC-COPD.

(A) UMAP plot depicting nine macrophage clusters.

(B) Proportions of these macrophage clusters in normal and tumor tissues.

(C) Bubble plot illustrating TGFβ1-receptor interactions between malignant cells and tumor-associated macrophages.

(D-E) Spatial feature plots displaying IL4I1 expression and macrophage distribution.

(F) Bubble plot demonstrating interactions between macrophages and both malignant and immune cells.

(G) IL4I1 mRNA expression in THP-1 cells treated with TGF-β1 at different doses or for different durations.

(H) Western blot images.

(I) LGALS9 mRNA expression in THP-1 cells treated with TGF-β1 at different doses or for different durations.

(J) Gal-9 secretion in THP-1 cells treated with TGF-β1 at different doses or for different durations.

(K) Spatial feature plots highlighting IL4I1 expression, as well as $CD8^+$ T cell and TAM distribution in LC-COPD.

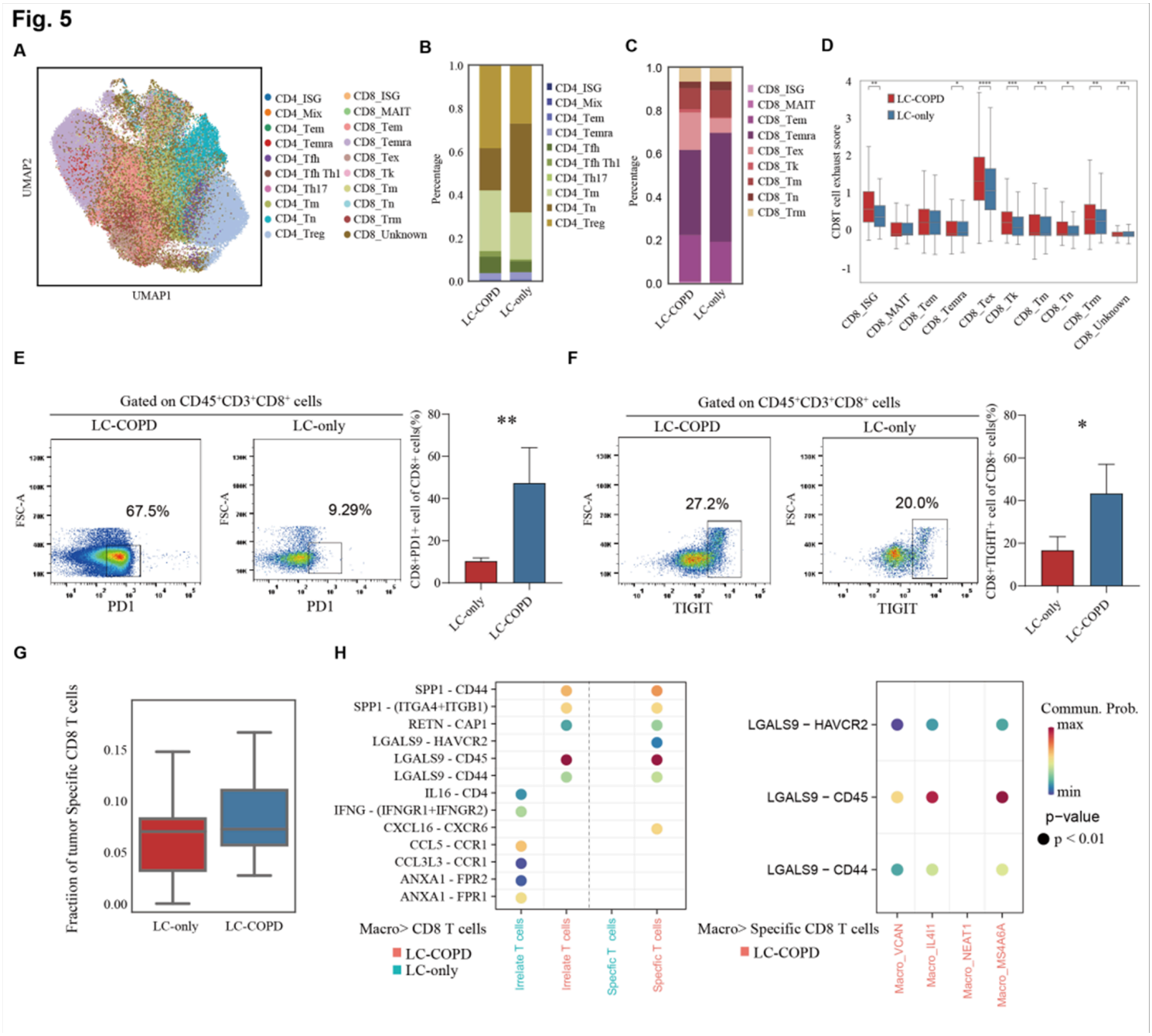


Figure 5

IL4I1 macrophages influence CD8$^+$ T cell exhaustion and tumor-specific responses in LC-COPD.

(A) UMAP plot of T cells, visualized as 20 distinct clusters.

(B–C) Comparison of cell fractions among CD4$^+$ T cell and CD8$^+$ T-cell subtypes between NSCLC patients with (LC-COPD) and without COPD (LC-only).

(D) Box plot illustrating the distribution of exhaustion scores among CD8$^+$ T cells.

(E–F) Representative flow cytometry plots depicting PD1^{+}CD8^{+} T cells and TIGIT^{+}CD8^{+} T cells, along with quantitative comparisons between LC-COPD and LC-only (student's t-test).

(G) Box plot of the fraction of tumor-specific CD8^{+} T cells in LC-COPD versus LC-only.

(H) Bubble plot showing interactions between macrophages and CD8+ T cells.

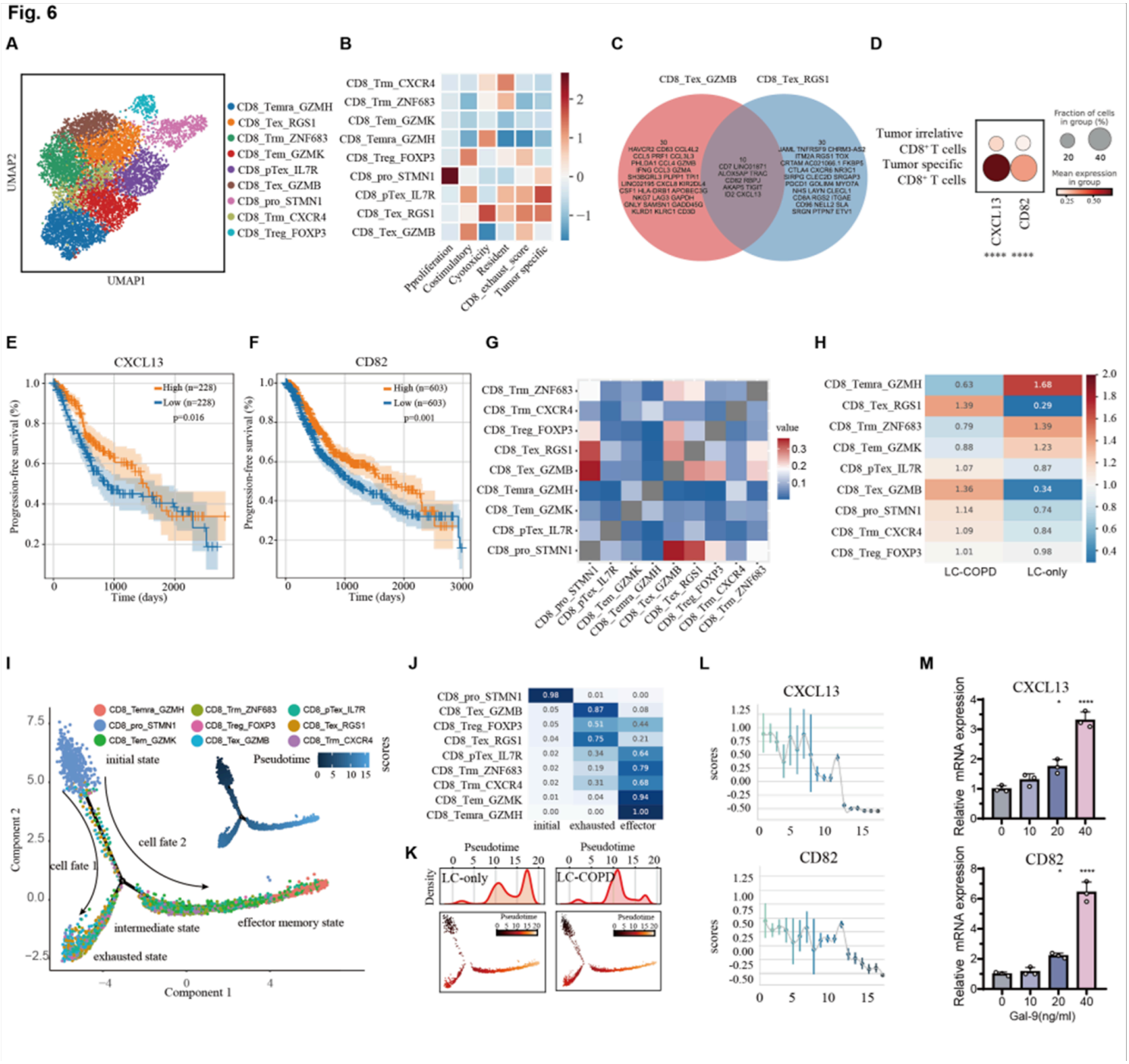


Figure 6

Characterization and functional analysis of tumor-specific CD8^{+} T cells in NSCLC with and without COPD

(A) UMAP plot of tumor-specific CD8^{+} T cells, colored by nine clusters.

(B) Heatmap showing the scores of six functional pathways.

(C) Venn diagram indicating the intersection of the top 40 marker genes in two Tex (exhausted) subsets.

(D) Bubble plot showing expression of CXCL13 and CD82 in tumor-specific versus tumor-unrelated $CD8^+$T cells.

(E–F) Survival analysis showing significant differences in progression-free-survival (PFS) between high and low expression of CXCL13 or CD82.

(G) Heatmap depicting the transition of tumor-specific $CD8^+$ T cells quantified by STARTRAC-tran indices.

(H) Heatmap of relative enrichment of tumor-specific $CD8^+$ T cells comparing NSCLC with COPD to those without COPD.

(I) Pseudotime trajectory for tumor-specific $CD8^+$ T cells, generated with Monocle (right), and a cell density plot illustrating the distribution of nine subtypes along the pseudotime axis (left).

(J) Heatmap of relative enrichment for each of the nine tumor-specific $CD8^+$ T-cell clusters in different states.

(K) Pseudotime plots of tumor-specific $CD8^+$ T cells in LC-only (left) versus LC-COPD (right), alongside cell density plots displaying the distribution across the pseudotime (top).

(L) Pseudotime plot demonstrating how CXCL13, and CD82 expression levels correlate with the transition of tumor-specific $CD8^+$ T cells.

(M) CXCL13 and CD82 mRNA expression in human $CD8^+$ T cells isolated from peripheral blood mononuclear cells treated with Gal-9 at different doses.

Supplementary Files

This is a list of supplementary files associated with this preprint. Click to download.

- TableS1.xlsx
- TableS5.xlsx
- TableS24.xlsx
- SupplementaryMethods.docx
- Supplementary.docx
- Graphabstract.docx